Science Advances
AAAS

advances.sciencemag.org/cgi/content/full/4/7/eaat6378/DC1

Supplementary Materials for

Ultrathin graphdiyne film on graphene through solution-phase van der Waals epitaxy

Xin Gao, Yihan Zhu, Ding Yi, Jingyuan Zhou, Shishu Zhang, Chen Yin, Feng Ding, Shuqing Zhang, Xiaohui Yi, Jizheng Wang, Lianming Tong*, Yu Han*, Zhongfan Liu*, Jin Zhang*

*Corresponding author. Email: jinzhang@pku.edu.cn (J.Z.); zfliu@pku.edu.cn (Z.L.); yu.han@kaust.edu.sa (Y.H.); tonglm@pku.edu.cn (L.T.)

Published 6 July 2018, *Sci. Adv.* **4**, eaat6378 (2018)
DOI: 10.1126/sciadv.aat6378

This PDF file includes:

Supplementary Materials and Methods

EXPERIMENTAL DETAILS

Graphene growth and transfer (*34*)

The graphene was grown on electrochemically polished copper foil (Alfa-Aesar, No. 46365) in a low-pressure chemical vapor deposition (LPCVD) system. The growth was carried out under the flow of H_2 and CH_4 (100:1 in volume) at 1020 ℃ for 40 min. The as-prepared continuous graphene films were transferred onto SiO_2/Si substrates, using poly (methyl methacrylate) (PMMA)-assisted wet method for graphdiyne (GDY) growth and Raman spectroscopy characterization. The graphene was grown on both sides of copper foils, and one side of the graphene used for GDY growth was spin coated with PMMA and baked at 120 °C for 10 min. Then, the other side of the sample was exposed to O_2 plasma for 5 min to remove the graphene. Subsequently, the 1M $FeCl_3$ solution was applied to etch the copper away. Then, the free-standing PMMA/graphene membrane floating on the surface of the etching solution was thoroughly washed with deionized water for several times, and then transferred onto SiO_2/Si substrates. After drying, the PMMA was carefully dissolved with hot acetone at 170 °C, yielding continuous graphene film on substrates.

Preparation of HEB (*19*)

Hexakis [(trimethylsilyl)ethynyl] benzene (TMS-HEB) was synthesized according to the reported synthetic route. TMS-HEB monomers (3.3 mg) were dissolved into 50 mL dichloromethane (CH_2Cl_2) solvent. Then, 50 μL tetrabutylammonium fluoride (1 M in tetrahydrofuran) was added into above-mentioned TMS-HEB solution. After stirring at 0 ℃ for 15 min under an argon atmosphere, hexakisbenzene (HEB, 0.1 mM in dichloromethane) was obtained, which served as the precursor solution of the coupling reaction and was used immediately.

COMPUTATIONAL DETAILS

First-principles calculations were performed using density functional theory (DFT) method implemented in the Vienna Ab-initio Simulation Package (VASP) code (*35*) to

obtain the energy variation during the synthesis of GDY. The generalized gradient approximation with the Perdew-Burke-Ernzerhof (GGA-PBE) type exchange-correlation functional and the projector augmented wave (PAW) method (*36*) were adopted in all calculations as well as the Tkatchenko-Scheffler (TS) method (*37*) for the vdW corrections. Spin polarized calculations were considered for all models. The plane-wave energy cutoff was fixed at 400 eV. The climbing-image nudged elastic band (cNEB) method (*38*) was exploited to locate the transition states during the process of deprotonation. The convergence of energy and force were set as 10^{-4} eV and 10^{-2} eV/Å (0.05 eV/Å for cNEB calculations), respectively. The preferential adsorption configurations of ABC-stacked tri-layer GDY flake on single-layer graphene (in Fig. 2) were searched by simulated annealing using the Metropolis Monte Carlo method and DREIDING force fields, unsaturated edge sites passivated by hydrogen. The adsorption configuration with lowest energy was then optimized by self-consistent charge density functional tight-binding methods with dispersion (Lennard-Jones potential) (SCC-DFTB-D).

CHARACTERIZATION

Characterization of morphology and structure was carried out by optical microscopy, scanning electron microscopy (Hitachi S-4800 operated at 2 kV). XPS measurement was conducted with Kratos Axis Ultra-DLD spectrophotometer using monochromatic Al X-ray at low pressures of 5×10^{-9} to 1×10^{-8} Torr. Raman spectra and confocal micro-PL measurements were conducted on Horiba HR800 Raman system with a laser excitation wavelength of 514.5 nm, spot size ~1 μm.

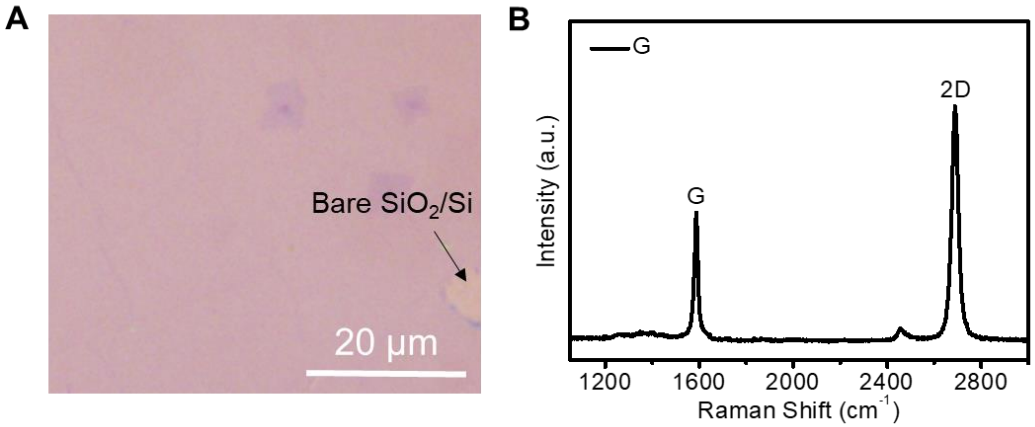

Fig. S1. Optical image and corresponding Raman spectrum of graphene film on SiO_2/Si substrate. Optical image (A) and corresponding Raman spectrum (B) of graphene film on SiO_2/Si substrate

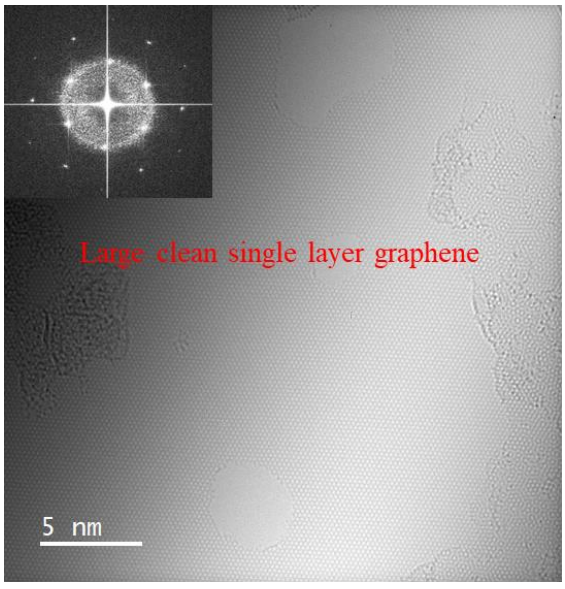

Fig. S2. HRTEM image of graphene substrate.

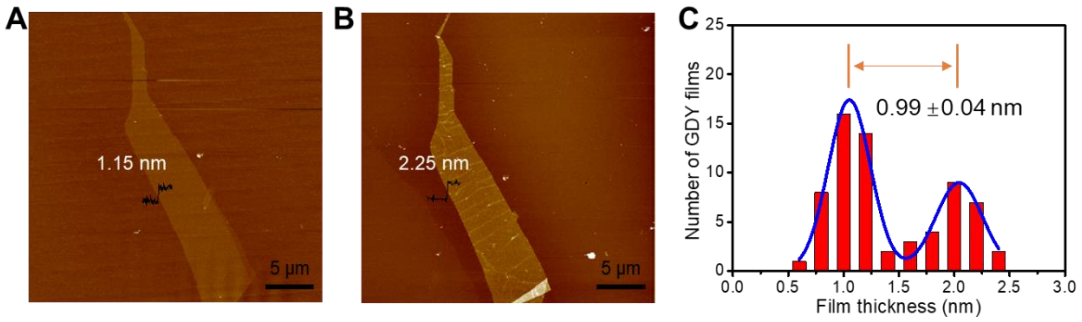

Fig. S3. Thickness analysis of as-grown GDY on graphene through a solution-phase vdW epitaxial strategy. Atomic force microscope (AFM) images of (A) a few-layered graphene sample mechanically exfoliated on a 300 nm SiO2/Si substrate and (B) after in-situ growth GDY on it. The same colour bar was used in (A) and (B). (C) AFM thickness histogram (red bars) and its Gaussian fitting (blue lines). A total of 66 independent samples are considered in the histogram.

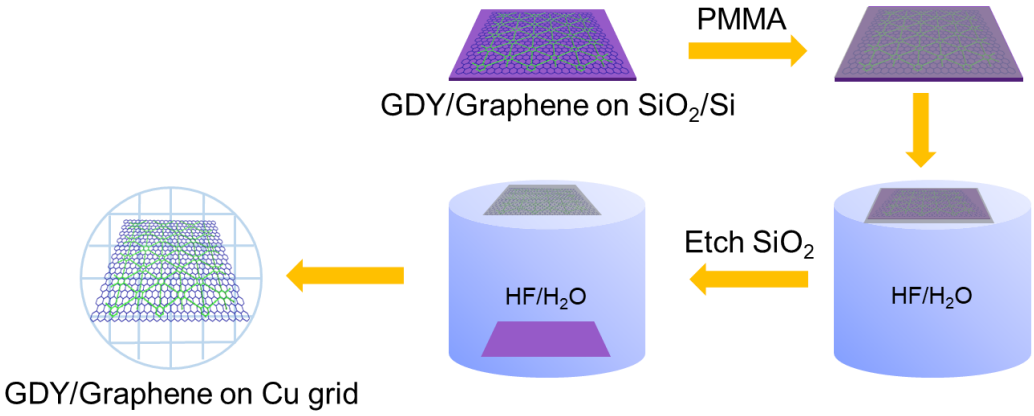

Fig. S4. The transfer process of the as-prepared GDY/graphene film from SiO_2/Si substrate to copper grid.

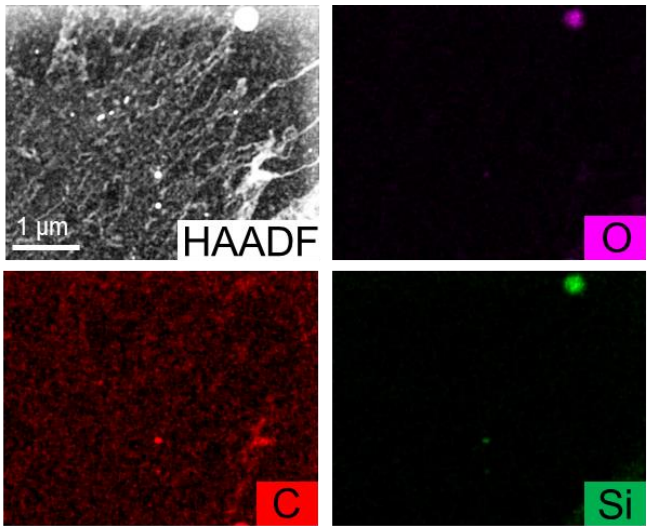

Fig. S5. Scanning TEM image and energy-dispersive x-ray spectroscopy elemental mapping images of C, O, and Si for GDY/graphene.

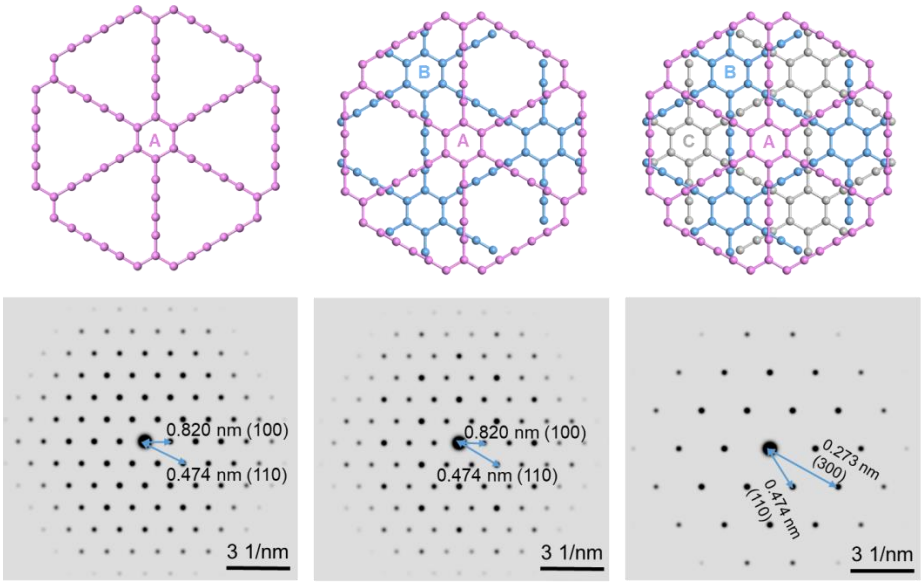

Fig. S6. GDY models with AA, AB, and ABC stacking modes and corresponding simulated SAED patterns of the stacking models.

	AA-stacked	AB-stacked	ABC-stacked
Binding Energy (meV/atom)	39.4	46.5	46.6
Binding Energy (kJ/mol)	3.802	4.487	4.496
Binding Energy (meV/nm^2)	792.5	935.3	937.3

Fig. S7. Calculated optimal binding energy of AA-, AB-, and ABC-stacked GDY structural models.

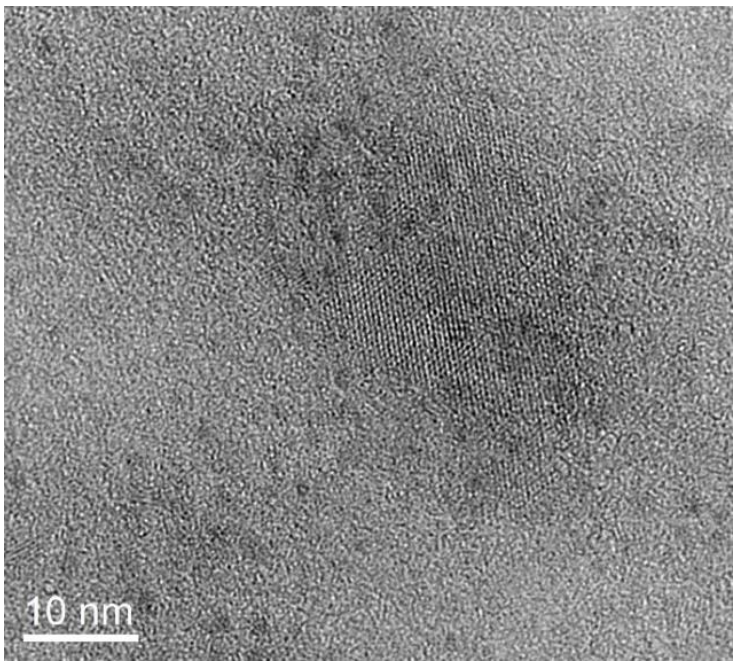

Fig. S8. As-grown GDY/graphene vdW heterostructure at high resolution.

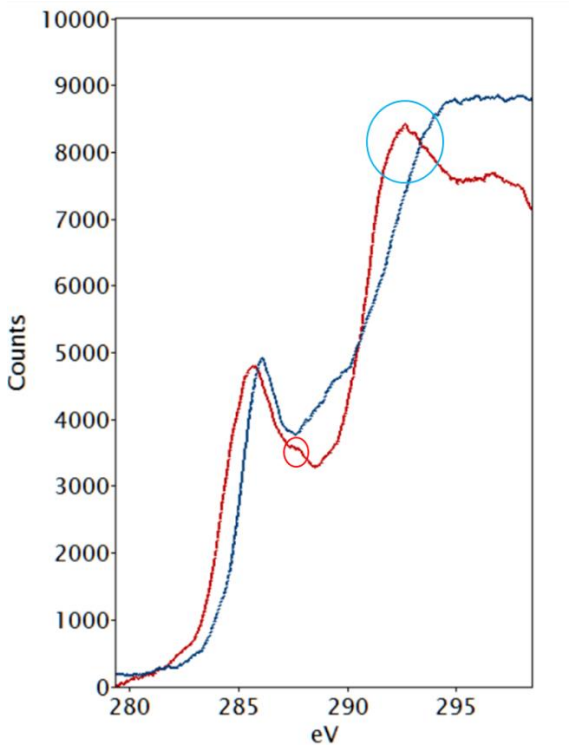

Fig. S9. Monochromated core-loss EELS spectra of GDY/graphene film collected under the (low-loss and core-loss) dual EELS mode. The core-loss EELS spectra was thus corrected by the zero-loss-peak (ZLP) in the low-loss spectra. Blue curve: carbon film as a reference; Red curve: GDY on Graphene. Typical sp^2 carbon 1s-π* features are 285.9 eV (blue) and 285.7 eV (Red). The shoulder in the red curve can be assigned to the sp carbon 1s-π* feature (marked by red circle, 287.1 eV) (*39*). The enhanced 1s-σ* feature in the blue circle is possibly caused by the presence of polymer used for transferring the 2D materials.

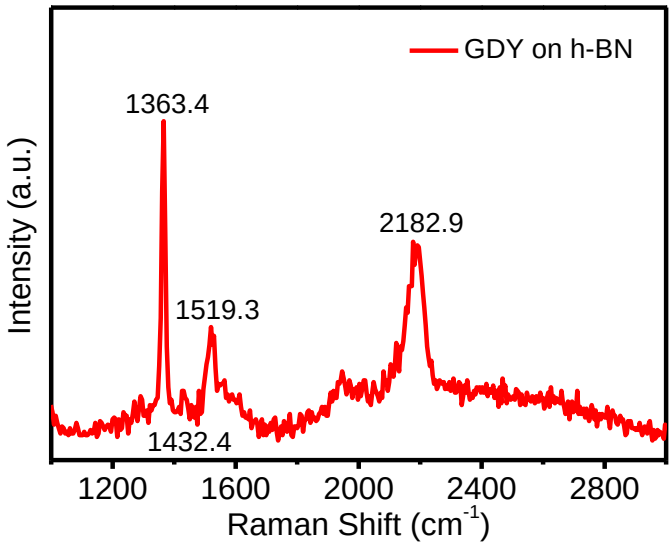

Fig. S10. Raman spectrum of GDY grown on h-BN substrate.

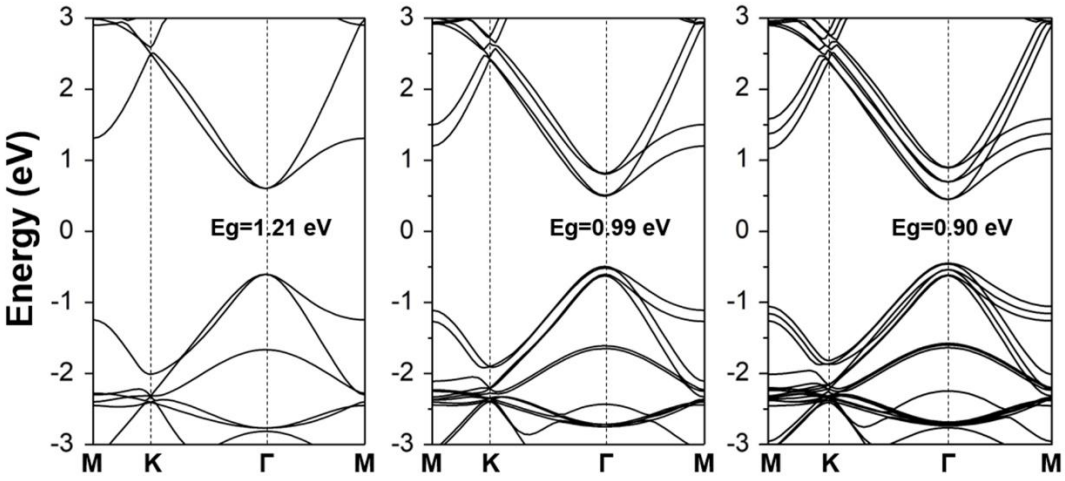

Fig. S11. Hybrid functional HSE06 predicted band structures and band gaps (Eg) for monolayer, bilayer, and trilayer GDY.

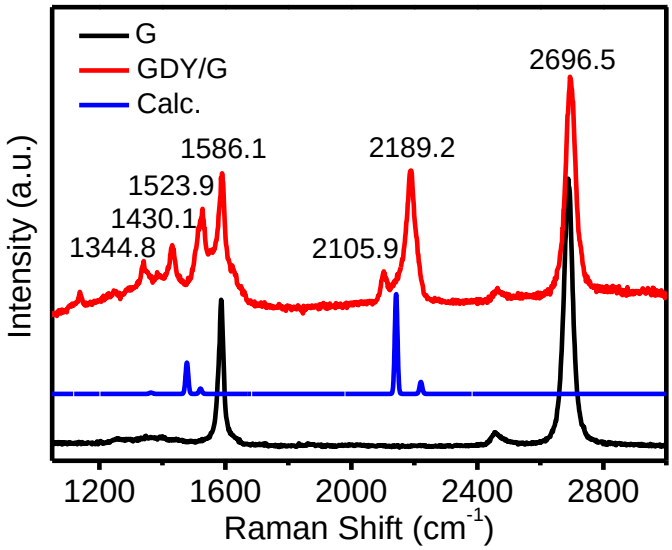

Fig. S12. Typical Raman spectra of GDY grown on graphene (red) with a reference blank graphene on SiO_2/Si substrate (black) and the calculated Raman spectra (*29*) of GDY (blue). In details, the G″ band (centered at 1344.8 cm^{-1}) is ascribed to the scissoring vibration of atoms in benzene ring; The G′ band (centered at 1430.1cm^{-1}) is the vibrations of C-C bonds between *sp*- and sp^2- hybridized carbon atoms; The G peak (centered at 1523.9 cm^{-1}) comes from stretching of aromatic bonds like in graphene (G_g), but the wavenumber and intensity of this mode ought to be relatively small in the alkyne-rich 2D systems, suggesting the successful introduction of acetylenic linkages in as-prepared GDY; The Y band (centered at 2105.9 cm^{-1}) and Y′ band (centered at 2189.2 cm^{-1}) are both ascribed to the stretching of triple bonds, where the vibrations of different triple bonds are in-phase belonging to Y, and different triple bonds are out-of-phase in Y′.

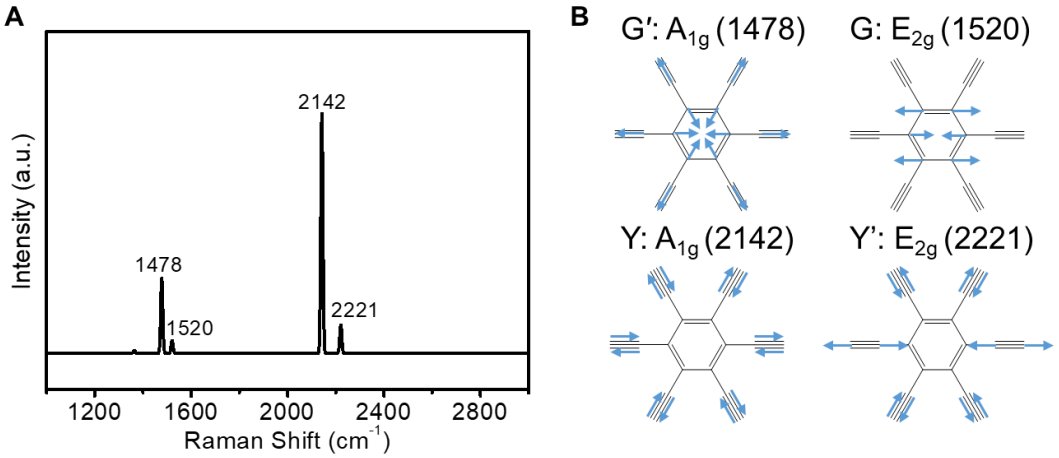

Fig. S13. Raman spectrum and corresponding vibrational modes of GDY. (A) Predicted Raman spectrum (*29*). (B) Atomic motions of intense Raman-active modes, in which the blue arrows show the motion directions of the main contributors.

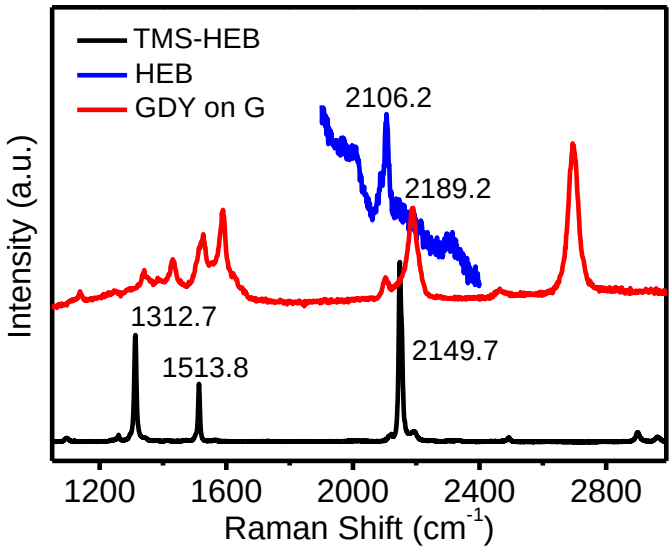

Fig. S14. Raman spectra of HEB monomer (blue), TMS-HEB monomer (black), and GDY (red).

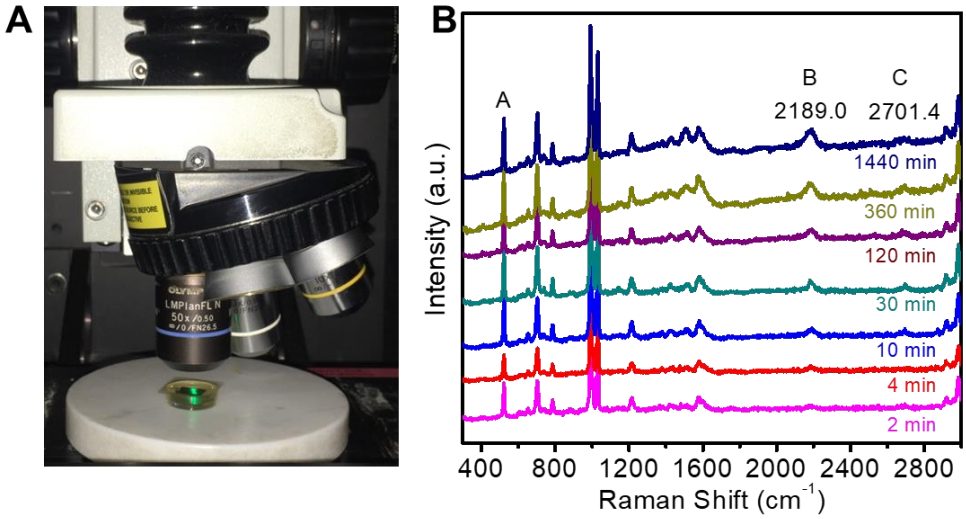

Fig. S15. In situ Raman spectroscopy to detect the change of the Y′ peak in GDY, which is a Raman-active peak from the stretching of C≡C triple bonds. (A) Optical image of the experimental setup. (B) Raman spectra change in the in-situ growth process at room temperature. An obvious Y′ peak appeared in a short reaction time (<4 minutes), indicating a rapid rate at the initial stage of homocoupling reaction**.**

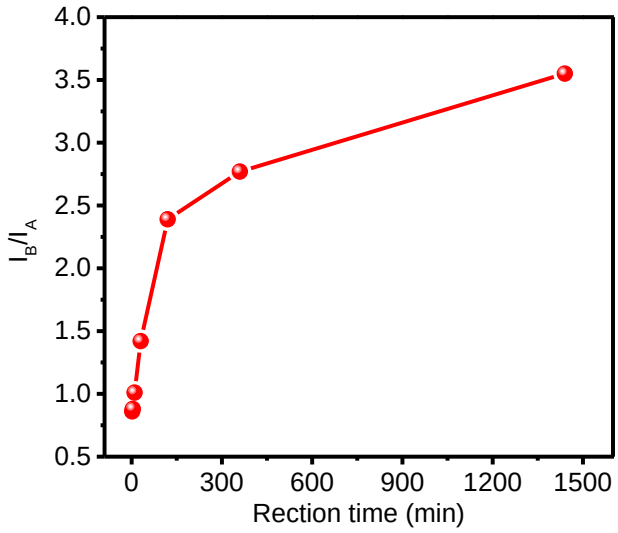

Fig. S16. The intensity of typical Y′ (2189.0 cm^{-1}) peak as a function of reaction time, using the peak (520.7 cm^{-1}) from Si substrate for intensity normalization. The intensity of Y′ peak has a significant enhancement with increasing time, showing that the terminal alkynes (HEB monomers) coupled quickly with each other to form an alkynyl-contained carbon network structure. However, the reaction rate decreaed with increasing reaction time, which results from the lower solubility and the lower reactivity of the enlarged alkynyl-contained carbon network structure.

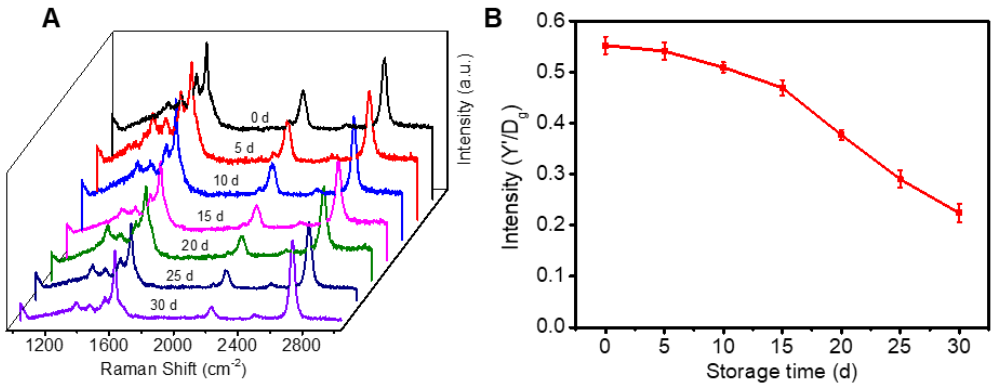

Fig. S17. Raman spectra taken from the same sample after being stored in air for several days. (A) Raman spectra taken from the same sample after being stored in air for several days. (B) Plot of the intensity ratio of Y′ and $2D_g$ change as storage time. After being stored in air for 10 days, intensity of Y′still kept at a high level, exhibiting an air-stability. Further analysis established that the ratio of Y′ and $2D_g$ decreased

from ~0.55 to ~0.47 after being stored in air for 15 days, but it still kept at a high level. After being stored in air for the subsequent 15 days, the ratio of Y′ and $2D_g$ showed an obvious decreasing tendency (from ~0.47 to 0.22), which maybe results from the reaction of *sp*- carbon with adsorbed O_2 on GDY.

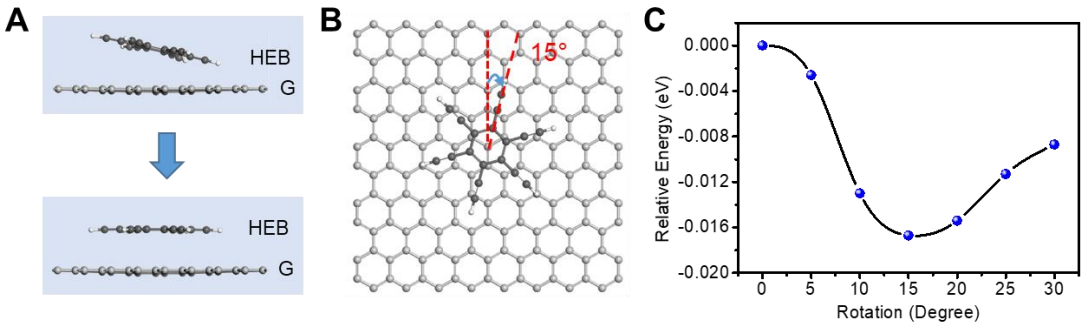

Fig. S18. Theoretical simulations of adsorption behavior of HEB on graphene. The absorbed HEB molecule shows a flat-lying geometry parallel to the graphene surface due to the vdW binding of 1.47 eV per molecule.

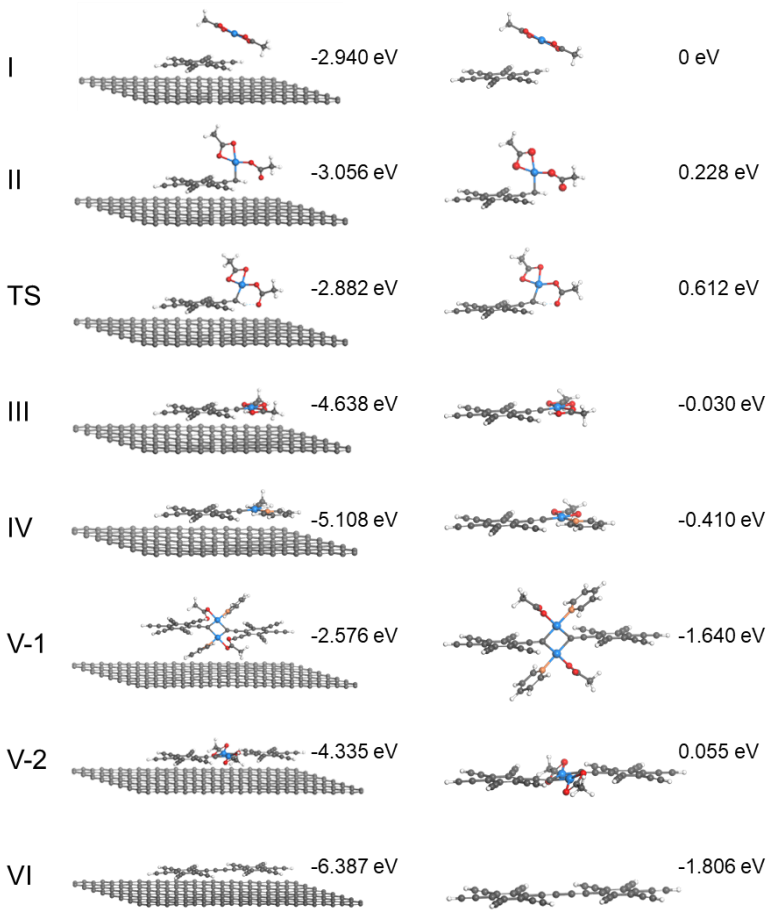

Fig. S19. Detailed structures and relative energy of I to VI and TS (Cu: blue; O: red; C: gray; N: orange; and H: white). Left: on graphene; Right: in solution. V-1 is a more stable intermediate (lower in energy than V-2) in solution, but V-2 is a more stable intermediate on graphene, which leads to an in-plane coupling reaction of HEB on graphene.

In detail, the catalytic cycle starts with the coordination of the terminal alkyne to copper acetate (I) to form intermediate II. In intermediate II, two kinds of new interactions are established. One of them is between one of the acetate groups and the proton of the incoming alkyne, and another one is between the proximal carbon atom of the alkyne and the copper center. The particular arrangement of ligands in intermediate II facilitates the proton transfer between the alkyne (HEB) and the pending acetate. From II to III is the process of HEB deprotonation, which is the rate-determine steps in Eglinton coupling reaction (*40*). Once III is formed, the reaction proceeds by replacing

the newly formed acetic acid moiety by a pyridine molecule (IV). Then dimerization of IV formed binuclear alkynyl-bridged complex V. Finally, we can get the final coupling product by a fast bimetallic reductive elimination process (V to VI).

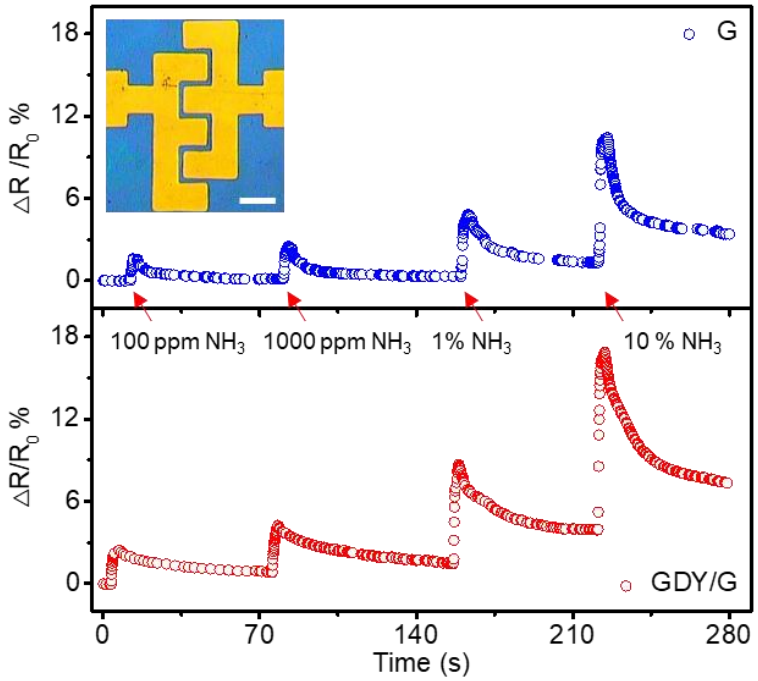

Fig. S20. NH_3 detection at room temperature and atmospheric pressure. Percentage increase in graphene and GDY/grpahene sheets resistance as a function of time for various NH_3 concentrations. Scale bar, 300 μm.

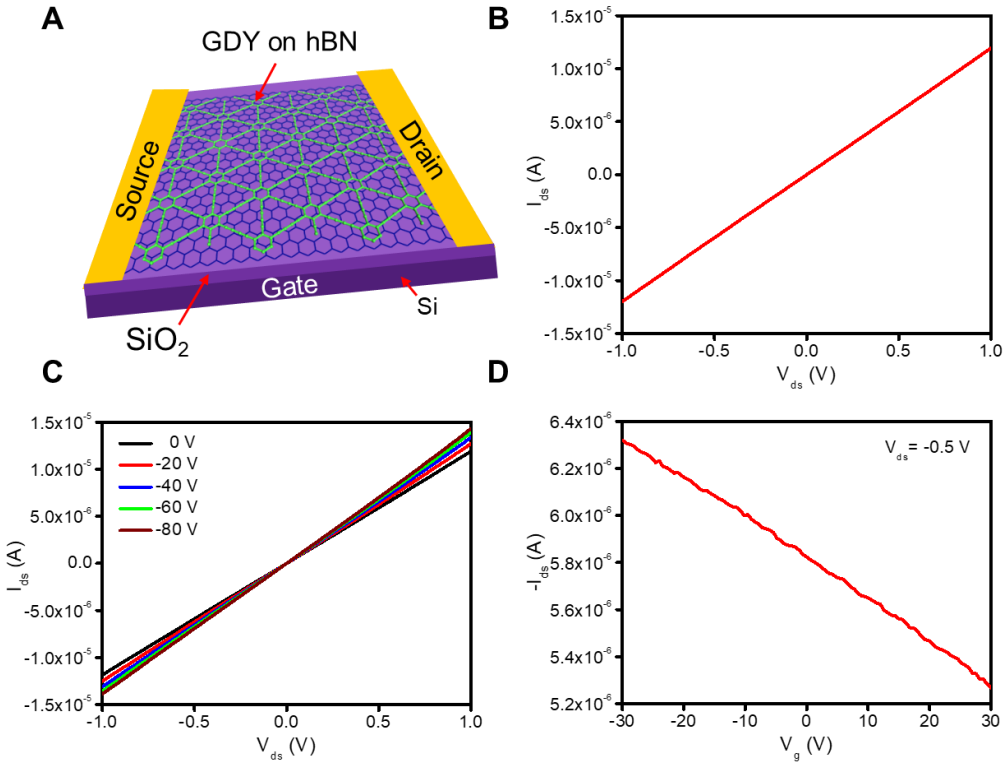

Fig. S21. Evaluation of the electrical property of the as-synthesized GDY. (A) Schematic view of GDY transistor. (B) I-V_{ds} characteristic for the device. (C) I_{ds}-V_{ds} curves recorded under various Vg biases from 0 V to -80 V. (D) Transport characteristic curve of the device at V_{ds} = -0.5 V.

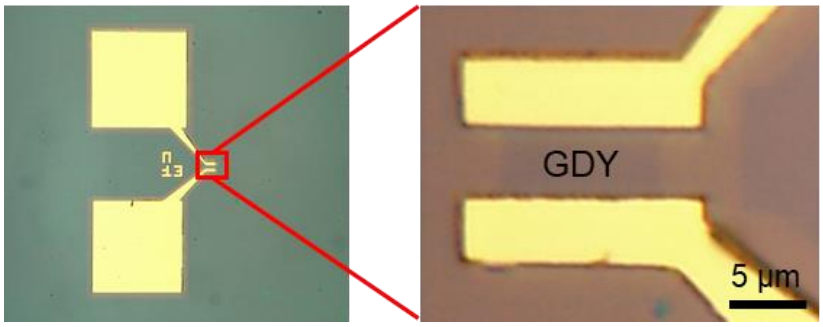

Fig. S22. OM images of the device in fig. S20.

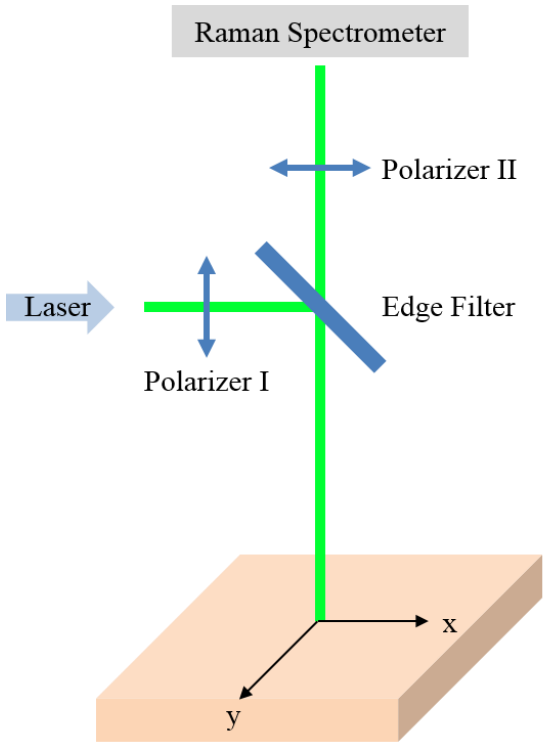

Fig. S23. The optical layout of the polarized Raman measurement.